# In-Plane Coassembly Route to Atomically Thick Inorganic–Organic Hybrid Nanosheets

**Xiaodong Zhang,[†,§] Qinghua Liu,[‡,§] Lingju Meng,[†] Hui Wang,[†] Wentuan Bi,[†] Yanhua Peng,[‡] Tao Yao,[‡] Shiqiang Wei,[‡,*] and Yi Xie[†,*]**

[†]Hefei National Laboratory for Physical Science at Microscale, University of Science and Technology of China, Hefei, Anhui 230026, People's Republic of China and [‡]National Synchrotron Radiation Laboratory, University of Science and Technology of China, Hefei, Anhui 230029, People's Republic of China. [§]These authors contributed equally to this work.

**ABSTRACT** Control over the anisotropic assembly of small building blocks into organized structures is considered an effective way to design organic nanosheets and atomically thick inorganic nanosheets with nonlayered structure. However, there is still no available route so far to control the assembly of inorganic and organic building blocks into a flattened hybrid nanosheet with atomic thickness. Herein, we highlight for the first time a universal in-plane coassembly process for the design and synthesis of transition-metal chalcogenide–alkylamine inorganic–organic hybrid nanosheets with atomic thickness. The structure, formation mechanism, and stability of the hybrid nanosheets were investigated in detail by taking the $Co_9S_8$–oleylamine ($Co_9S_8$–OA) hybrid nanosheets as an example. Both experimental data and theoretical simulations demonstrate that the hybrid nanosheets were formed by in-plane connection of small two-dimensional (2D) $Co_9S_8$ nanoplates *via* oleylamine molecules adsorbed at the side surface and corner sites of the nanoplates. X-ray absorption fine structure spectroscopy study reveals the structure distortion of the small 2D $Co_9S_8$ nanoplates that endows structural stability of the atomically thick $Co_9S_8$–OA hybrid nanosheets. The brand new atomically thick nanosheets with inorganic–organic hybrid network nanostructure will not only enrich the family of atomically thick 2D nanosheets but also inspire more interest in their potential applications.

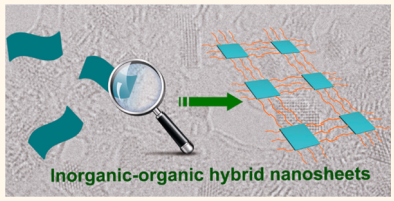


**KEYWORDS:** two-dimensional nanosheets · in-plane · coassembly · inorganic–organic hybrid · atomically thick

Self-assembly is a common phenomenon in nature and has long been studied by scientists for the design of a wide variety of complex and hierarchical structures artificially.[1,2] Understanding and controlling the underlying assembly process of small building blocks into organized structures will be beneficial to design and synthesize various novel structures with practical values.[3−6] In recent years, the self-assembly process in solution has been well-established, during which the small building blocks can be self-organized into types of structures, such as wires, sheets, and three-dimensional (3D) crystals, by balancing the attractive and repulsive forces.[7−9] For example, Tang *et al.* self-assembled the zero-dimensional (0D) CdTe nanoparticles into free-standing two-dimensional (2D) nanosheets to simulate the assembly of S-layer proteins experimentally.[8] However, self-assembly of small building blocks into the non-close-packed nanostructures is still a great challenge.

Since the discovery of graphene, great efforts have been made to synthesize the atomically thick free-standing 2D nanosheets with thickness under 1 nm, which can effectively combine novel microscopic electronic structures with macroscopic ultrathin, transparent, and flexible devices and are considered as the prototype materials for the study of the intrinsic 2D confinement effect.[10−12] The graphene and inorganic graphene analogues (IGA) with intrinsic layered structure can be easily obtained by exfoliation or peeling off process from their bulk counterparts.[13−16] Because of the lack of intrinsic driving force for 2D anisotropic growth, controlling assembly of small building blocks is considered to be an effective way to obtain the atomically thick nanosheets of the nonlayered structural inorganic materials and organic polymers.[17,18]

Recently, our group has successfully synthesized a series of free-standing inorganic nanosheets with atomic thickness, such as single-unit-cell-thick ZnSe[19] and $SnS_2$[20]

* Address correspondence to yxie@ustc.edu.cn, sqwei@ustc.edu.cn.

Received for review December 8, 2012 and accepted January 23, 2013.

**Published online January 23, 2013**
**10.1021/nn3056719**

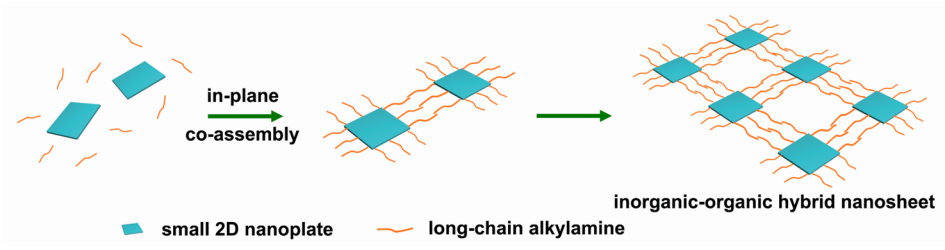


**Figure 1. Schematic illustration of the in-plane coassembly route to the inorganic−organic hybrid nanosheets with atomic thickness in the presence of long-chain alkylamine. Here we used the word "nanoplate" to name the small 2D nanostructure.**

nanosheets, as well as half-unit-cell-thick $Co_9Se_8$ nanosheets.[21] Their unique structures were studied by X-ray absorption fine structure spectroscopy (XAFS) and theoretical calculation. Thanks to the recent development of organic synthesis, a few atomically thick organic nanosheets have also been successfully prepared.[22,23] However, to the best of our knowledge, inorganic−organic hybrid nanosheets with atomic thickness have never been reported so far, although they are expected to show the synergy effect or totally new properties beyond the single inorganic and organic nanosheets.

To date, it is still a great challenge to prepare the atomically thick inorganic−organic hybrid nanosheets due to the lack of executable synthesis and assembly strategies. Previously, inorganic−organic hybrid nanosheets are generally attained by the layer-by-layer alternate assembly of the inorganic nanosheets and organic components, thus the thicknesses of the hybrid nanosheets are up to at least several nanometers.[17,24] It seems only possible to synthesize atomically thick inorganic−organic hybrid nanosheets by alternately connecting the inorganic and organic parts in a confined 2D space, due to the reduced surface energy and excellent structural stability in such a unique connecting way.

Besides the reduced surface energy and stabilized structure arising from the alkylamine adsorption on the metal atoms of nanoclusters, the adsorption energy between alkylamines and metal-compound nanoclusters heavily relies on the adsorption sites.[25−27] These facts give us inspiration that the alkylamine and metal compound nanoclusters could be assembled into the 2D inorganic−organic nanosheets by effectively controlling the kinds of alkylamine and metal-compound nanoclusters.

Herein, we highlight a universal pathway for the controlled synthesis of ultrathin transition-metal chalcogenide−alkylamine inorganic−organic hybrid nanosheets with atomic thickness by a unique in-plane coassembly strategy between small 2D transition-metal chalcogenide nanoplates and alkylamines with different lengths. As illustrated in Figure 1, long-chain alkylamine ($C_nH_{2n+x}NH_2$ with $n \geq 12$) can stabilize the small 2D nanoplates by adsorbing on the corner sites and side surface sites and then connect with each other in-plane to randomly assemble into the atomically thick inorganic−organic hybrid nanosheets in a confined 2D space. However, if a short-chain alkylamine ($C_nH_{2n+x}NH_2$ with $n \leq 8$) is used instead of the long-chain alkylamines during the reaction process, the small 2D nanoplates cannot be effectively stabilized and would aggregate to form a 3D nanostructure ultimately. Numerous experiments show that different kinds of transition-metal chalcogenide−alkylamine ($M_xT_y$−alkylamine, M = Co, Ni, Fe; T = S, Se) hybrid nanosheets could be successfully obtained by in-plane coassembly of small 2D nanoplates and long-chain alkylamine (such as oleylamine, 1-octadecylamine, 1-hexadecylamine, 1-tetradecylamine, 1-dodecylamine, *etc.*). However, only the 3D transition-metal chalcogenide nanostructures could be obtained during the same reaction condition while the long-chain alkylamine was replaced with short-chain alkylamine (such as 1-octanamine, butylamine, propylamine, *etc.*) (see details in Supporting Information S3−S6). All of the results indicate that the in-plane coassembly strategy is a universal method for the preparation of transition-metal chalcogenide−alkylamine inorganic−organic hybrid nanosheets with atomic thickness by controlling the species of inorganic and organic components. The structure, formation mechanism, and stability of the hybrid nanosheets will be investigated in detail for the first time by taking the $Co_9S_8$−oleylamine ($Co_9S_8$−OA) hybrid nanosheets as an example.

## RESULTS AND DISCUSSION

The composition of the as-synthesized nanosheets was first investigated by Fourier transform infrared (FT-IR) spectra and thermogravimetric (TG) analysis (Figure S1). The IR spectra analysis indicates the existence of oleylamine molecules in the synthetic nanosheets, and detailed TG analysis indicates that the weight content of oleylamine in the nanosheets is as high as 41.7%. To go further, the inorganic component of the synthetic nanosheets was studied by the energy-dispersive spectroscopy (EDS) spectra (Figure S2) and X-ray photoelectron spectroscopy (XPS) spectra (Figure S3). It is shown that the synthetic nanosheets are composed of Co and S, with the Co/S molar ratio of about 1.10 yielded from EDS and 1.13 from XPS, respectively, both close to the stoichiometric ratio (1.12) of $Co_9S_8$. The peak of N element in the XPS can

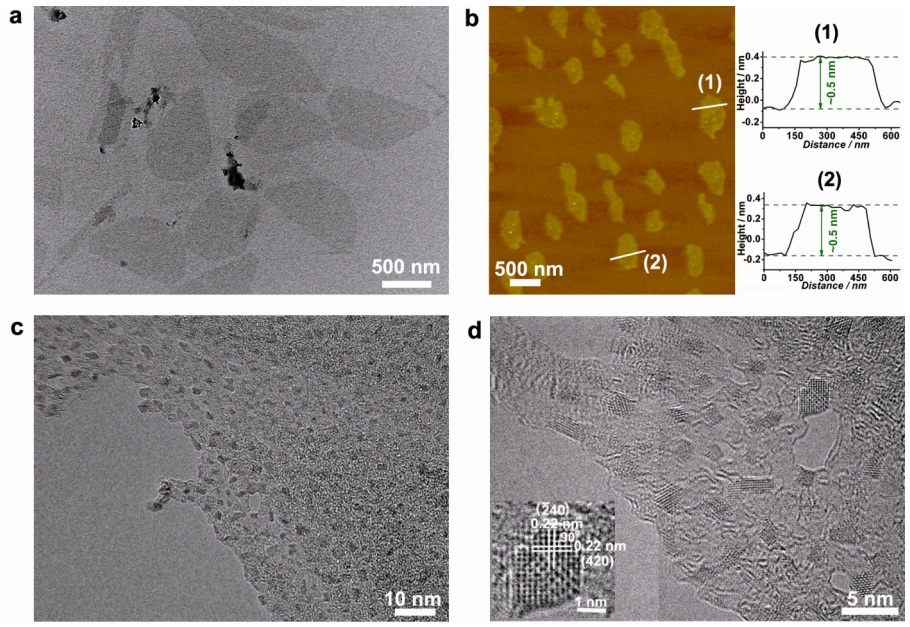


**Figure 2. (a) TEM image of the ultrathin $Co_9S_8$–OA hybrid nanosheets. (b) Tapping-mode AFM image of the $Co_9S_8$–OA ultrathin nanosheets, showing the single layer of only about 0.5 nm in thickness. (c,d) HRTEM images of the $Co_9S_8$–OA nanosheet with different magnification. Inset of (d) is the HRTEM image of a typical 2D $Co_9S_8$ nanoplate.**

be ascribed to the presence of oleylamine in the synthetic nanosheets.

Figure 2a is the TEM image of the as-obtained $Co_9S_8$–OA hybrid nanosheets, from which the large-area free-standing nanosheets with length up to 1 $\mu$m and width of about 500 nm are clearly visible. Moreover, the nearly transparent feature of the nanosheets indicates their ultrathin thickness. Seen from Figure 2a, besides the free-standing nanosheets, there are also tiny amounts of large nanoparticles, but up to 95% of the small 2D $Co_9S_8$ nanoplates are assembled into nanosheets as estimated from the TEM image. The as-prepared hybrid nanosheets can be dispersed in cyclohexane to form a stable suspension without any aggregation for several weeks. The ultrathin nanosheets possess a certain degree of physical integrity and remain the sheet morphology even after strong ultrasound treatment for several hours and can be easily assembled into large-area films by vacuum filtration with tunable thickness, structure integrity, and flexibility for further practical applications (Figure S15).

It is well-known that tapping-mode atomic force microscopy (AFM) is the most important and direct tool for measuring the height of 2D graphene and graphene analogues with atomic thickness. As shown in the AFM image (Figure 2b), two randomly measured as-obtained hybrid nanosheets have nearly the same thickness of only about 0.5 nm, which is just a half-unit-cell-thick $Co_9S_8$ crystal structure (Figure S16). To further study the microscopic structure of the hybrid nanosheet, high-resolution TEM (HRTEM) measurements of a typical hybrid nanosheet were carried out. It can be clearly seen that the nanosheets are made up of randomly arranged small 2D $Co_9S_8$ nanoplates, which should be connected with each other by oleylamine molecules (Figure 2c,d and Figure S5). HRTEM images of further large magnification show the small nanoplates with diameters ranging from 1 to 2 nm and the same exposed surface plane. As can be clearly seen from the inset of Figure 2d, the lattice fringes of 0.22 nm correspond to the {420} lattice plane of the $Co_9S_8$ crystal structure and suggest the exposure of the *XY* plane in the 2D nanoplates. The HRTEM image of a typical large nanoparticle generated during the fabrication process, as shown in Figure S4, reveals its single-crystalline nature and shows the same {420} lattice plane as in the small 2D $Co_9S_8$ nanoplate. This provides evidence that the bulk nanoparticles are formed by the oriented attachment of the small 2D nanoplates. The Raman spectra (Figure S6) of the synthetic nanosheets show a blue shift of about 7 $cm^{-1}$ with respect to the spectra of $Co_9S_8$ bulk samples, indicating a phonon confinement effect in the $Co_9S_8$–OA hybrid nanosheets due to their unique half-unit-cell-thick $Co_9S_8$ crystal structure.[20]

All of the above results demonstrate that the atomically thick $Co_9S_8$–OA inorganic–organic hybrid nanosheets have been successfully obtained. However, there is still a question unresolved: How does the seemingly isolated small 2D $Co_9S_8$ nanoplates and oleylamine make up the ultrathin nanosheets with flattened morphology and atomic thickness?

In order to answer this question, we carried out theoretical simulations to understand the underlying formation mechanism of the free-standing $Co_9S_8$–OA hybrid nanosheets. On the basis of the size and thickness of the $Co_9S_8$ 2D nanoplates obtained from the experimental data, we built a 2 × 2 two-dimensional

**a**

| Coverage | $\Delta E_{ads}$ (eV/mol) |
|---|---|
| $T_1$ | 0.45 |
| $T_2$ | 0.98 |
| $S_1$ | -0.05 |
| $S_2$ | -0.56 |
| $C_1$ | -0.87 |
| $C_2$ | -1.12 |

**b**

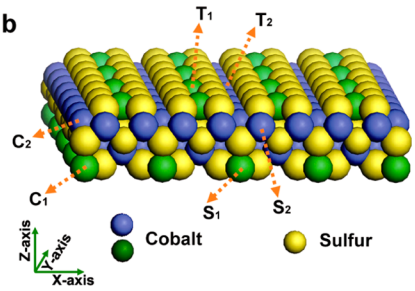


**Figure 3. (a) Table of calculated adsorption energy of oleylamine molecules adsorbed on different sites of $Co_9S_8$ nanoplate. T, top surface sites; S, side surface sites; C, corner sites; 1 and 2, different adsorption cases. (b) Schematic illustration of the different Co atom sites in a four-atom thick $Co_9S_8$ nanoplate.**

unit cell containing eight atoms per plane to mimic the 2D $Co_9S_8$ nanoplate that was four atoms thick.

In this model, the Co sites of the four-atom thick $Co_9S_8$ nanoplate can be mainly divided into three types: top surface sites (T), side surface sites (S), and corner sites (C), and each Co site can be further divided into two types for their different coordinations (Figure 3b). We calculated the adsorption energy between the connection of three different Co sites and oleylamine molecules to estimate the most stable connection model. The adsorption energy $\Delta E_{ads}$ is defined as follows:

$$\Delta E_{ads} = E_{tot}(NP + OA) - E_{tot}(NP) - E_{tot}(OA)$$

where $E_{tot}(NP + OA)$, $E_{tot}(NP)$, and $E_{tot}(OA)$ are the total energies of oleylamine molecules adsorbing on the $Co_9S_8$ nanoplate, the $Co_9S_8$ nanoplate alone, and oleylamine molecules alone, respectively. The negative value of $\Delta E_{ads}$ implies that adsorption is exothermic; therefore, the more negative the $\Delta E_{ads}$ is, the more stable the model will be. As shown in Figure 3a, it is noticeable that the binding energies of oleylamine adsorbing on the corner sites and side surface sites of the $Co_9S_8$ 2D nanoplate are lower than the value of adsorbing on the top surface sites. Specifically, the binding energy has a positive value when oleylamine was adsorbed on the top surface sites of the nanoplate and turns to a negative value when adsorbed on the corner or side surface sites. At the corner sites, the binding energy has the most negative value. These results indicate that oleylamine molecules energetically prefer to adsorb on the corner sites and side surface sites of Co atoms of the 2D $Co_9S_8$ nanoplate, rather than to adsorb on the top surface sites of Co atoms of the 2D nanoplate. Hence, through oleylamine molecules, the small 2D nanoplates with atomic thickness could be in-plane connected with each other to form inorganic–organic hybrid nanosheets with flattened morphology and atomic thickness. By taking butylamine ($C_4H_9NH_2$) as an example, we further studied the adsorption energy between the small 2D $Co_9S_8$ nanoplate and short-chain alkylamine by theoretical simulations. As shown in Table S1, the adsorption energies of butylamine at all surface sites are positive, indicating the endothermic adsorption between butylamine and $Co_9S_8$ nanoplate that prohibits the formation of inorganic–organic hybrid nanosheets through mutual connection.

To study the local atomic arrangements of the synthetic ultrathin $Co_9S_8$–OA hybrid nanosheets, we conducted X-ray absorption fine structure spectroscopy measurement, which is a powerful local structural characterization method for its element specificity and good sensitivity to the short-range order (typically several Å).[28] The extended XAFS (EXAFS) $k^3\chi(k)$ functions and corresponding Fourier transforms (FTs) at Co *K*-edges of both the synthetic $Co_9S_8$–OA nanosheets and bulk $Co_9S_8$ sample are shown in Figure 4a,b. Clearly, the $k^3\chi(k)$ oscillation curve for the $Co_9S_8$–OA nanosheets exhibits a slight decrease in frequency and a remarkable reduction in amplitude between *k* regions of 4–10 $Å^{-1}$ compared with the bulk counterpart. In the FT curves (Figure 4b), two prominent peaks at 1.83 and 3.31 Å corresponding to Co–S and Co–Co coordinations, respectively, can be observed for bulk $Co_9S_8$. However, in the FT curve of the nanosheet, one can find that the first peak decreases in intensity and shifts toward a lower R position (1.75 Å), although the second peak of Co–Co coordination is almost invariable. It should be noted that the shift of the first peak can be mainly due to the presence of Co–N coordination because the Co–N bond length is shorter than the Co–S one. Quantitative curve fittings of the EXAFS spectra were performed, and the results are summarized in Table S2. For the ultrathin $Co_9S_8$–OA nanosheets, the coordination number and bond length of Co–N are 1.1 and 2.10 Å, respectively, indicating the presence of oleylamine adsorbed on the cobalt atoms of the hybrid nanosheets. Further, the surface Co–S bond length of 2.30 Å for the nanosheet is contracted compared with that (2.37 Å) for bulk, while the next nearest Co–Co bond lengths of 2.54 and 3.60 Å are a little elongated. On the basis of these structural parameters, the schematic structure models of the 2D $Co_9S_8$ nanoplate of four atoms thick were built as shown in Figure 4c, in which the changed bond lengths were labeled. Clearly, both the Co–S and Co–Co distances in the $Co_9S_8$ nanoplate exhibited noticeable structural distortions as compared with the bulk sample. For the unique half-unit-cell structure of the $Co_9S_8$ nanoplate, the loss of neighbor coordinating atoms will trigger the structure relaxation of the nanoplate to minimize

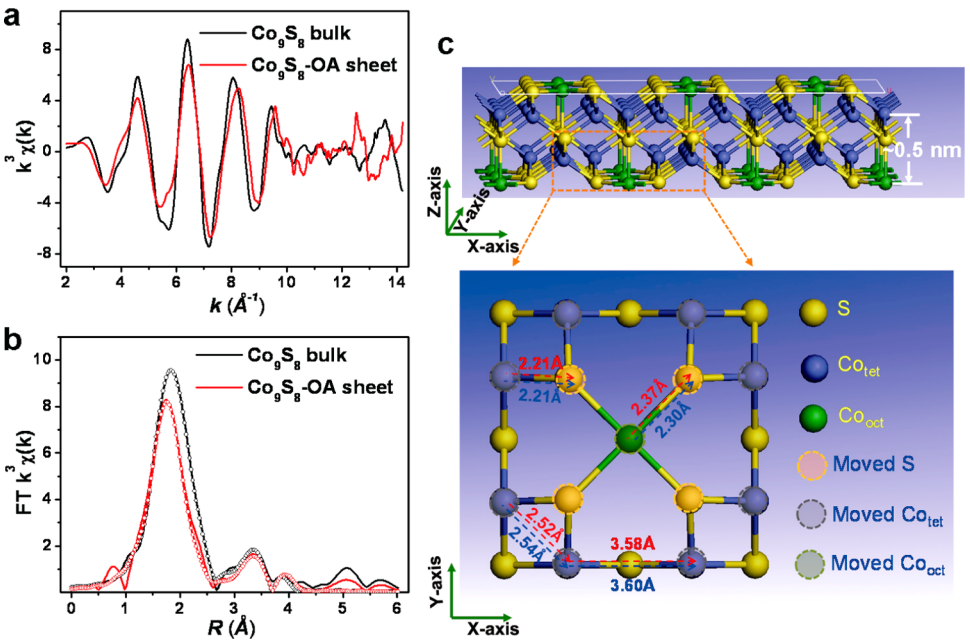


**Figure 4. (a) Co *K*-edge extended XAFS oscillation function $k^3\chi(k)$ and (b) corresponding Fourier transforms. (c) Structure changes between the unrelaxed and relaxed 2D $Co_9S_8$ nanoplate model.**

the surface energy, which consequently endows the stability of the inorganic–organic hybrid nanostructure. In addition, the surface distortion of the $Co_9S_8$ nanoplate revealed by XAFS not only stabilizes the hybrid nanosheet structure but also influences their electronic structure and brings on novel physical properties.

Generally speaking, the atomically thick nanosheets can be mainly divided into two category: inorganic nanosheets and organic nanosheets.[13,23] In recent years, though a few inorganic–organic hybrid nanosheets have been reported, organic molecules in those materials are often located among the inorganic nanosheets to stabilize their lamellar structure and show a thickness up to at least several nanometers.[17,24] The atomically thick inorganic–organic hybrid nanosheets should have inorganic and organic building blocks alternately arranged in a confined 2D space with stable structure. The as-obtained transition-metal chalcogenide–alkylamine hybrid nanosheets reported here will be the first case of artificial inorganic–organic hybrid nanosheets with atomic thickness. In addition, the universal in-plane coassembly strategy could be further expanded to synthesize other kinds of inorganic–organic hybrid nanosheets with atomic thickness.

## CONCLUSION

In summary, we have developed a universal method for the synthesis of a series of inorganic–organic hybrid nanosheets by in-plane coassembly of small 2D transition-metal chalcogenide nanoplates and alkylamines with different length. Detailed experimental results on $Co_9S_8$–OA nanosheets show that the ultrathin nanosheets with 2D alternately arranged inorganic–organic hybrid network structure have been successfully synthesized. In addition, the synthetic nanosheets show flattened morphology with a thickness of about 0.5 nm, corresponding to a half-unit-cell $Co_9S_8$ crystal structure. The formation mechanism of the $Co_9S_8$–OA nanosheets was studied by the theoretical simulations. It is revealed that oleylamine tends to adsorb on the corner sites and side surface sites of the small 2D $Co_9S_8$ nanoplates, which favors the in-plane coassembly strategy. Furthermore, the Co–N coordination detected by XAFS gives direct evidence of oleylamine adsorbed on the cobalt atoms in the hybrid nanosheets. The surface distortion revealed by XAFS endows excellent stability of the atomically thick $Co_9S_8$ nanoplate and will generate new electronic structure for further study. This report for the first synthesis of the atomically thick inorganic–organic hybrid nanosheets not only offers a universal in-plane coassembly synthetic method but also enriches the family of atomically thick nanosheets.

## METHODS

**Preparation of Ultrathin $Co_9S_8$-Alkylamine/$CoSe_2$-Alkylamine Inorganic–Organic Hybrid Nanosheets.** The ultrathin $Co_9S_8$–oleylamine ($Co_9S_8$–OA) inorganic–organic hybrid nanosheets were synthesized by a solvothermal method, in which the solvent was the mixture of benzyl alcohol and oleylamine. In a typical procedure, 0.091 g of $CoC_2O_4 \cdot 2H_2O$ (0.5 mmol) and 0.037 g of $CH_3CSNH_2$ (TAA) (0.5 mmol) were added into the mixed solvent of benzyl alcohol (30 mL) and oleylamine (6 mL) in succession. After strongly stirring for about 1 h, the mixed solution was

transferred into a 45 mL Teflon cup and heated in a sealed autoclave at 180 °C for 20 h. Upon cooling to room temperature, the precipitate was washed with the mixed solvent of cyclohexane and ethanol several times and dried under vacuum at 60 °C for further analysis. In this reaction, if we replaced the TAA with $SeO_2$ and kept the other reaction parameters unchanged, the $CoSe_2$–OA inorganic–organic hybrid nanosheets would be obtained. To go further, if oleylamine was replaced by other long-chain alkylamines ($C_nH_{2n+x}NH_2$ with $n \geq 12$), a series of $Co_9S_8$–alkylamine and $CoSe_2$–alkylamine hybrid nanosheets would be obtained. However, if only short-chain alkylamine existed in the reaction, 3D nanostructures would be obtained. See details in Supporting Information (S3 and S4).

**Preparation of Other Transition-Metal Chalcogenide–Alkylamine Inorganic–Organic Hybrid Nanosheets.** The ultrathin $FeSe_2$–alkylamine, $NiSe_2$–alkylamine, Fe–S–alkylamine, and Ni–S–alkylamine hybrid nanosheets can also be obtained by similar reaction conditions of $Co_9S_8$–alkylamine/$CoSe_2$–alkylamine hybrid nanosheets just with the reagent sources changed. See details in Supporting Information (S5 and S6).

**Calculation Method.** The first-principles density functional theory (DFT) calculations were performed using a plane wave basis set with the projector augmented plane-wave (PAW) method.[29–32] The exchange-correlation interaction is described within the generalized gradient approximation (GGA) in the form of PW91.[33,34] The energy cutoff is set to 400 eV, and the atomic positions are allowed to relax until the energy and force are less than $10^{-4}$ eV and $10^{-3}$ eV/Å, respectively. We use a $2 \times 2$ two-dimensional unit cell containing eight atoms per plane to mimic the 2D $Co_9S_8$ nanoplate that is four atoms thick. Each 2D $Co_9S_8$ nanoplate model consists of four atomic planes and is separated by a vacuum region of 15 Å. The compared calculations of bulk $Co_9S_8$ were performed within a supercell constructed from a standard unit cell of $Co_9S_8$ lattice.

*Conflict of Interest:* The authors declare no competing financial interest.

*Acknowledgment.* The research was financially supported by National Basic Research Program of China (2009CB939901), Chinese Academy of Science (XDB01020300), and National Natural Science Foundation of China (11079004 and 90922016).

*Supporting Information Available:* Detailed experimental section, additional information of the as-prepared inorganic–organic hybrid nanosheets, and detailed XAFS fitting results. This material is available free of charge *via* the Internet at http://pubs.acs.org.

## REFERENCES AND NOTES

1. Lehn, J.-M. Toward Self-Organization and Complex Matter. *Science* **2002**, *295*, 2400–2403.
2. Ringsdorf, H.; Schlarb, B.; Venzmer, J. Molecular Architecture and Function of Polymeric Oriented Systems: Models for the Study of Organization, Surface Recognition, and Dynamics of Biomembranes. *Angew. Chem., Int. Ed. Engl.* **1988**, *27*, 113–158.
3. Whitesides, G. M.; Boncheva, M. Beyond Molecules: Self-Assembly of Mesoscopic and Macroscopic Components. *Proc. Natl. Acad. Sci. U.S.A.* **2002**, *99*, 4769–4774.
4. Nie, Z.; Petukhova, A.; Kumacheva, E. Properties and Emerging Applications of Self-Assembled Structures Made from Inorganic Nanoparticles. *Nat. Nanotechnol.* **2010**, *5*, 15–25.
5. Gao, B.; Arya, G.; Tao, A. R. Self-Orienting Nanocubes for the Assembly of Plasmonic Nanojunctions. *Nat. Nanotechnol.* **2012**, *7*, 433–437.
6. Xia, Y.; Nguyen, T. D.; Yang, M.; Lee, B.; Santos, A.; Podsiadlo, P.; Tang, Z.; Glotzer, S. C.; Kotov, N. A. Self-Assembly of Self-Limiting Monodisperse Supraparticles from Polydisperse Nanoparticles. *Nat. Nanotechnol.* **2011**, *6*, 580–587.
7. Li, C.; Numata, M.; Bae, A.-H.; Sakurai, K.; Shinkai, S. Self-Assembly of Supramolecular Chiral Insulated Molecular Wire. *J. Am. Chem. Soc.* **2005**, *127*, 4548–4549.
8. Tang, Z.; Zhang, Z.; Wang, Y.; Glotzer, S. C.; Kotov, N. A. Self-Assembly of CdTe Nanocrystals into Free-Floating Sheets. *Science* **2006**, *314*, 274–278.
9. Breen, T. L.; Tien, J.; Olivers, S. R. J.; Hadzic, T.; Whitesides, G. M. Design and Self-Assembly of Open, Regular, 3D Mesostructures. *Science* **1999**, *284*, 948–951.
10. Feng, J.; Sun, X.; Wu, C.; Peng, L.; Lin, C.; Hu, S.; Yang, J.; Xie, Y. Metallic Few-Layered $VS_2$ Ultrathin Nanosheets: High Two-Dimensional Conductivity for In-Plane Supercapacitors. *J. Am. Chem. Soc.* **2011**, *133*, 17832–17838.
11. Feng, J.; Peng, L.; Wu, C.; Sun, X.; Hu, S.; Lin, C.; Dai, J.; Yang, J.; Xie, Y. Giant Moisture Responsiveness of $VS_2$ Ultrathin Nanosheets for Novel Touchless Positioning Interface. *Adv. Mater.* **2012**, *24*, 1969–1974.
12. Wang, X.; Zhi, L.; Mullen, K. Transparent, Conductive Graphene Electrodes for Dye-Sensitized Solar Cells. *Nano Lett.* **2008**, *8*, 323–327.
13. Coleman, J. N.; Lotya, M.; O'Neill, A.; Bergin, S. D.; King, P. J.; Khan, U.; Young, K.; Gaucher, A.; De, S.; Smith, R. J.; *et al.* Two-Dimensional Nanosheets Produced by Liquid Exfoliation of Layered Materials. *Science* **2011**, *331*, 568–571.
14. Ramakrishna Matte, H. S. S.; Gomathi, A.; Manna, A. K.; Late, D. J.; Datta, R.; Pati, S. K.; Rao, C. N. R. $MoS_2$ and $WS_2$ Analogues of Graphene. *Angew. Chem., Int. Ed.* **2010**, *49*, 4059–4062.
15. Zeng, Z.; Yin, Z.; Huang, X.; Li, H.; He, Q.; Lu, G.; Boey, F.; Zhang, H. Single-Layer Semiconducting Nanosheets: High-Yield Preparation and Device Fabrication. *Angew. Chem., Int. Ed.* **2011**, *50*, 11093–11097.
16. Ren, L.; Qi, X.; Liu, Y.; Hao, G.; Huang, Z.; Zou, X.; Yang, L.; Li, J.; Zhong, J. Large-Scale Production of Ultrathin Topological Insulator Bismuth Telluride Nanosheets by a Hydrothermal Intercalation and Exfoliation Route. *J. Mater. Chem.* **2012**, *22*, 4921–4926.
17. Schliehe, C.; Juarez, B. H.; Pelletier, M.; Jander, S.; Greshnykh, D.; Nagel, M.; Meyer, A.; Foerster, S.; Kornowski, A.; Klinke, C.; *et al.* Ultrathin PbS Sheets by Two-Dimensional Oriented Attachment. *Science* **2010**, *329*, 550–553.
18. Kissel, P.; Erni, R.; Schweizer, W. B.; Rossell, M. D.; King, B. T.; Bauer, T.; Götzinger, S.; Schlüter, A. D.; Sakamoto, J. A Two-Dimensional Polymer Prepared by Organic Synthesis. *Nat. Chem.* **2012**, *4*, 287–291.
19. Sun, Y.; Sun, Z.; Gao, S.; Cheng, H.; Liu, Q.; Piao, J.; Yao, T.; Wu, C.; Hu, S.; Wei, S.; *et al.* Fabrication of Flexible and Freestanding Zinc Chalcogenide Single Layers. *Nat. Commun.* **2012**, *3*, 1057.
20. Sun, Y.; Cheng, H.; Gao, S.; Sun, Z.; Liu, Q.; Liu, Q.; Lei, F.; Yao, T.; He, J.; Wei, S.; *et al.* Freestanding Tin Disulfide Single-Layers Realizing Efficient Visible-Light Water Splitting. *Angew. Chem., Int. Ed.* **2012**, *51*, 8727–8731.
21. Zhang, X.; Zhang, J.; Zhao, J.; Pan, B.; Kong, M.; Chen, J.; Xie, Y. Half-Metallic Ferromagnetism in Synthetic $Co_9Se_8$ Nanosheets with Atomic Thickness. *J. Am. Chem. Soc.* **2012**, *134*, 11908–11911.
22. An, Q.; Chen, Q.; Zhu, W.; Li, Y.; Tao, C.; Yang, H.; Li, Z.; Wan, L.; Tian, H.; Li, G. A Facile Method for Preparing One-Molecule-Thick Free-Standing Organic Nanosheets with a Regular Square Shape. *Chem. Commun.* **2010**, *46*, 725–727.
23. Sakamoto, J.; van Heijst, J.; Lukin, O.; Schlüter, A. D. Two-Dimensional Polymers: Just a Dream of Synthetic Chemists? *Angew. Chem., Int. Ed.* **2009**, *48*, 1030–1069.
24. Son, J. S.; Wen, X.-D.; Joo, J.; Chae, J.; Baek, S.-i.; Park, K.; Kim, J. H.; An, K.; Yu, J. H.; Kwon, S. G.; *et al.* Large-Scale Soft Colloidal Template Synthesis of 1.4 nm Thick CdSe Nanosheets. *Angew. Chem., Int. Ed.* **2009**, *48*, 6861–6864.
25. Wang, X.; Zhuang, J.; Peng, Q.; Li, Y. A General Strategy for Nanocrystal Synthesis. *Nature* **2005**, *437*, 121–124.
26. Park, J.; An, K.; Hwang, Y.; Park, J.-G.; Noh, H.-J.; Kim, J.-Y.; Park, J.-H.; Hwang, N.-M.; Hyeon, T. Ultra-Large-Scale Syntheses of Monodisperse Nanocrystals. *Nat. Mater.* **2004**, *3*, 891–895.
27. Li, Z.; Peng, X. Size/Shape-Controlled Synthesis of Colloidal CdSe Quantum Disks: Ligand and Temperature Effects. *J. Am. Chem. Soc.* **2011**, *133*, 6578–6586.
28. Crozier, E. D. A Review of the Current Status of XAFS Spectroscopy. *Nucl. Instrum. Methods Phys. Res., Sect. B* **1997**, *133*, 134–144.

29. Blöchl, P. E. Projector Augmented-Wave Method. *Phys. Rev. B* **1994**, *50*, 17953–17979.
30. Kresse, G.; Furthmüller, J. Efficient Iterative Schemes for *Ab Initio* Total-Energy Calculations Using a Plane-Wave Basis Set. *Phys. Rev. B* **1996**, *54*, 11169–11186.
31. Kresse, G.; Furthmüller, J. Efficiency of *Ab-Initio* Total Energy Calculations for Metals and Semiconductors Using a Plane-Wave Basis Set. *Comput. Mater. Sci.* **1996**, *6*, 15–50.
32. Kohn, W.; Sham, L. J. Self-Consistent Equations Including Exchange and Correlation Effects. *Phys. Rev.* **1965**, *140*, A1133–A1138.
33. Perdew, J. P.; Wang, Y. Accurate and Simple Analytic Representation of the Electron-Gas Correlation Energy. *Phys. Rev. B* **1992**, *45*, 13244–13249.
34. Wang, Y.; Perdew, J. P. Correlation Hole of the Spin-Polarized Electron Gas, with Exact Small-Wave-Vector and High-Density Scaling. *Phys. Rev. B* **1991**, *44*, 13298–13307.